Automated Segmentation of Cells with IHC Membrane Staining

Elisa Ficarra, Andrea Acquaviva, Santa Di Cataldo, and Enrico Macii

Department of Control and Computer Engineering, Politecnico di Torino, Corso Duca degli Abruzzi 24, 10129 Torino ITALY, e-mail: elisa.ficarra@polito.it, andrea.acquaviva@polito.it, santa.dicataldo@polito.it (corresponding author), enrico.macii@polito.it.

Keywords Immunohistochemistry, tissue images, cell segmentation, cellular membrane segmentation, membrane staining, image processing, protein expression

Abstract

This work presents a fully-automated membrane segmentation technique for immunohistochemical tissue images with membrane staining, which is a critical task in computerized IHC. Membrane segmentation is particularly tricky in immunohistochemical tissue images because the cellular membranes are visible only in the stained tracts of the cell, while the unstained tracts are not visible. Our automated method provides accurate segmentation of the cellular membranes in the stained tracts and reconstructs the approximate location of the unstained tracts using nuclear membranes as a spatial reference. Accurate cell-by-cell membrane segmentation allows per cell morphological analysis and quantification of the target membrane proteins, that is fundamental in several medical applications such as cancer characterization and classification, personalized therapy design, and for any other applications requiring cell morphology characterization. Experimental results on real datasets from different anatomical locations demonstrate the wide applicability and high accuracy of our approach in the context of IHC analysis.

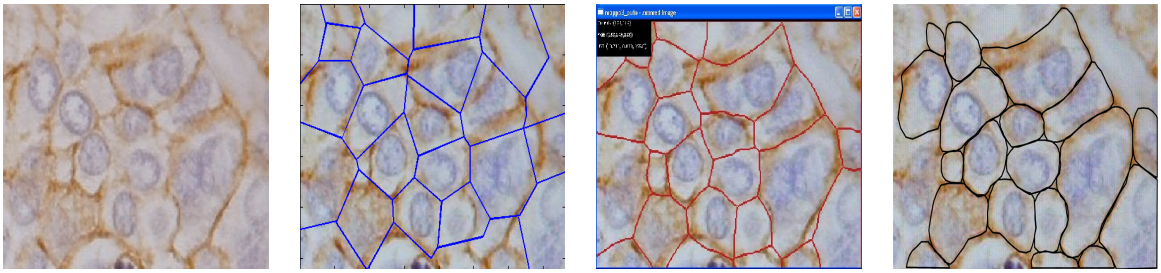

(a) (b) (c) (d)

Figure 1: a: example of immunohistochemical tissue image; b: membrane approximation obtained through standard Voronoi tessellation; c: membrane approximation obtained through our proposed labelling procedure (see Section 2.1); d: cellular membranes manually traced by a pathologist.

1 Introduction

Directly monitoring the activity of proteins that are involved in the genesis and development of multi-factorial genetic pathologies is a very useful diagnostic tool which leads to the assessment of the characteristics of the pathology. For example, *EGFR/erb-B* family of receptors plays an important role for a number of cancers, including lung, breast, colon, gastric cancer, etc.: quantifying and classifying the *EGFR* expression and activity with special regards to the assessment of the prevalence of *EGFR* mutations as well as to ligand-receptor interactions leads to new insights into the modulation of the receptor in individual carcinomas.

Moreover, the quantitative analysis of protein expression in situ in pathological tissues opens new opportunities for the design of novel targeted therapies through the definition of a group of potential candidates to protein family-inhibiting therapies. Thus, it is important to extract protein expression information by using methodologies that give quantifiable and standardized measurements [1].

One of the most prominent techniques in this field is immunohistochemistry (IHC) [2], that uses specific marked antibodies to stain proteins in situ, thus allowing the identification of many cell and sub-cell types that could be visualized by microscopy. The analysis of stains' intensity and distribution at the specific location of interest targeted by the receptors (i.e. nuclei, cellular membranes or cytoplasm of the cells, depending on the receptors) allows to extract localized and highly specific protein expression information that is extremely useful for the assessment of the pathology. [1].

In the last few years immunohistochemistry has acquired a central role in the field of pathology thanks to its several advantages over alternate bioimaging techniques (e.g. fluorescence in situ hybridization, FISH); these advantages include its wide availability, relatively low cost, easy and long preservation of the stained slides [3]. With the goal of making pathologic examinations less subjective, the widespread use of immunohistochemistry initially assisted pathologists only in making diagnoses, adding to or complementing morphological information with molecular information. More recently, it has been used to predict response to targeted therapy and to correlate protein and genetic expression data for improving therapies' accuracy [4] (see Fig. 1.a for an example of IHC tissue image).

This new role of IHC is placing new demands on the reproducibility, accuracy and specificity of the extracted information [5]. In fact IHC analysis has been traditionally performed by pathologists through direct visual inspection of micrographs of the specimens, which is extremely time-consuming, error-prone and highly affected by inter- as well as by intra-operator variability [6], [7]; only recently the growing demand for automatization is being addressed by the main providers of systems for digital pathology, with dedicated software integrated to the IHC acquisition systems [3], [8], [9].

As recently aknowledged by modern pathology, for maximum relevance immunohistochemistry should address per cell rather than per tissue analysis of the target proteins [10]: in fact, cells have been ultimately recognized as the fundamental units of behaviour in multiple molecular pathways at the basis of pathology and cancer biology, so that the relevant metric in cancer development relies on their specific individual phenotypes [10]. This implies that the analytes are assessed in identifiable individual cells rather than on average in the whole side of tissue, which is not compatible with traditional visual evaluation. For this purpose, there is a growing demand for automated techniques able to identify cell by cell the specific location of interest of the studied receptors.

In this paper we present an automated method for the cell-by-cell segmentation of cellular membranes in immunostained tissues, which is is a highly critical task, especially in chromogenic IHC.

The most challenging issue is related to the reconstruction of the membranes in the portions that are negative to the target receptors (i.e. where protein activity is not present), that are not revealed by the stain and then not visible. The lack of intensity or gradient magnitude variations in the unstained parts of the membranes as well as the staining heterogeneity that is instrinsic of IHC imaging invalidate segmentation methods detecting

intensity or gradient variations between the background and the pattern to be segmented [13]. Active contours approaches [14], [15], [16] overcome the problem of connecting broken contour lines by modeling the target pattern with a closed curve, but on the other hand they are extremely sensitive to initialization as well as to staining artifacts which may attract them far from the target membrane.

The largest amount of literature in the field of cellular membrane segmentation addresses fluorescence or confocal microscopy images, where most of the challenges are related to the nonuniformity of the fluorescence signal, which may create variations and gaps in the membrane continuity. Interesting approaches have been proposed in this field: [17] presented a method based on Voronoi regions with a metric controlled by local image properties; [18] recently presented a generalized version of the Subjective Surfaces technique, while [19] used iterative tangential voting to enhance the protein bound signal followed by evolving fronts.

Very fewer techniques deal with automated membrane segmentation in chromogenic IHC, where different challenges arise due to the presence of unstained portions of the tissues (i.e. where the cells are negative to the target receptor and the membranes are not visible at all) and to the noise generated by the superposition and diffusion of different stains over the sample. Most of the recent works have been proved to be effective with nuclear segmentation but do not address cellular membranes' segmentation [20], [21], [22] or are semi-automated in that they need a certain amount of user-intervention to add control points close to the target membrane boundary [23], [24]. Other recent works rely on elliptic approximation of the target membranes [25], [26], which does not reflect much the real morphology of several pathological tissues (see Fig. 1 for examples).

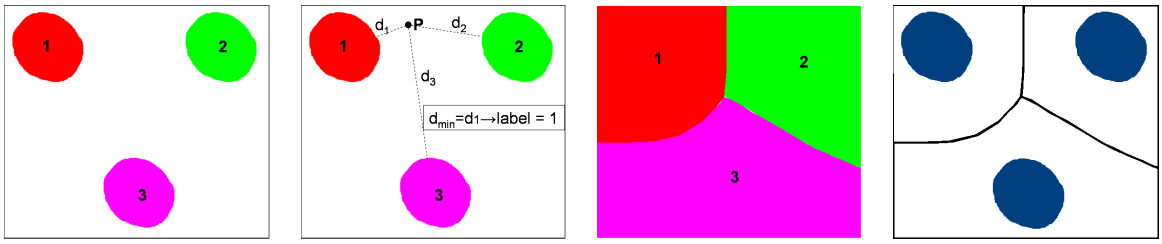

(a) (b) (c) (d)

Figure 2: Scheme of labelling procedure for the computation of approximate cell membranes. a: regions are initialized with the points enclosed by the nuclear membranes; each region is characterized by a region-label (1, 2 and 3 in this case) and represented by a different color; b: each point P in the image is given the label of the closest nuclear membrane (in this case, label=1); c: final labelled regions; d: approximate cell membranes obtained by outlining the labelled regions.

In this work we present a method that provides fully-automated segmentation of the cellular membranes in chromogenic IHC images, based on accurate detection of the stained tracts of the membranes and biologically realistic reconstruction of the unstained tracts using nuclear membranes as a spatial reference.

The paper is organized as follows. In Section 2 we describe our fully-automated procedure for cellular membrane segmentation. Section 3 reports the implementation details. In Section 4 we show experimental results which demonstrate the accuracy of our technique on real IHC images. Section 5 concludes the paper.

2 Materials and Methods

We analyzed histopathology images characterized by a blue stain (Hematoxylin, H) as background colour and a brown stain (Diaminobenzidine, DAB) revealing the areas of the tissue where the target receptor as well a ligand of the target receptor family is detected; nevertheless, as explained later in Section 2.2, our technique can be easily applied to IHC images with different histological stains. The images were acquired from different anatomical locations (i.e. lung, liver, prostate cancer tissue). In particular, our experimental dataset included eight specimens acquired by different patients with resolutions spanning from 0.15 to 0.6 μm/px and with membrane protein activation spanning from weak to very strong (see Section 4 and Table 2 for a complete characterization). All the images were analyzed by a pathologist, that provided manually segmented cellular membranes as ground truth to validate our procedure.

As outlined in Section 1, computer-aided immunohistochemical analysis ideally requires to identify cell by cell the regions of the tissue that are targeted by the analyte (e.g. nuclei, cytoplasm or cellular membranes); subsequently, it is possible to quantify the brown coloured areas at the identified location of interest.

In case of images with membrane staining, this implies the accurate cell-by-cell segmentation of the cellular membranes in the tissue, which is the task addressed by our technique.

The brown stain reveals only the parts of the membranes that are positive to the target receptors, therefore some cellular membranes may be totally unstained or either stained only in some tracts; only the stained tracts are visible and distinguishable from the background (see Fig. 1.a for an example). The amount of stained

membranes as well as the continuity of the staining over the membranes are related to the characteristics and to the status of the pathology [27] and are not predictable *a priori*; in particular, in order to be able to quantify the continuity if the staining in terms of amount of stained membrane the cellular membranes have to be reconstructed in both the stained (brown-colored) and the unstained tracts.

This calls for non-standard segmentation techniques working in absence of intensity information coming from the unstained membranes' tracts (either absolute or in terms of gradient variation) and able to adress staining inhomogeneity as well as non-predictable shape variations of the cells; these variations may be induced by the pathology or by the mechanical and thermal stresses of the sample preparation [10]. These critical conditions invalidate the efficiency of popular segmentation methods in Computer Vision such as watersheds [28] and active contours [29], as well as any other method based either on intensity variations or fixed geometrical models of the patterns.

In our technique we exploit the *detection of cellular membranes* by firstly reconstructing their approximate locations starting from nuclear membranes' profiles. This procedure, namely *computation of approximate cell membrane*, allows to locate the most likely profiles of the cellular membranes in the tissue. Then we detect the brown parts of the membranes through color filtering and we connect them to the approximate cellular membranes in those regions of the cell that are negative to receptor reaction and then not visible. This procedure, namely *detection of final cellular membranes*, reconstructs cellular membranes even in absence of intensity information, i.e. when membranes are partially or completely not visible in the image.

In the following subsections we provide a detailed description of our automated technique for membrane segmentation.

2.1 Computation of approximate cell membranes

Approximate cell membranes are closed curves that resemble the locations of cellular membranes in the tissue; they are computed following a *minimum distance* criterion from nuclear membranes' profiles. This assumption is the most realistic from a biological point of view since nuclei are generally located in the middle of the cell. On top of that, when the membrane is unstained, the location of the membrane can only be inferred from the position of the nuclei of the cells, therefore the *minimum distance* criterion appears to be the most reasonable solution.

As shown in Fig. 1.a, unlike cellular membranes, the profile of nuclei is completely visible and delineated, so it can be used as a reliable spatial reference for cellular membranes detection. In our previous works addressing the problem of nuclear segmentation we described and validated a fully-automated morphology-based method that provides nuclear profiles in IHC tissue images; in this work we used the nuclear profiles as a starting point for cellular membrane segmentation (see [30], [31] for more details).

Literature reports several well known tessellation approaches which partition a given image into regions including points that are closer to a specific object, for example Voronoi diagrams [32] and Delaunay triangulation [33]; these approaches have been used in many different biological fields including models of cell growth as well as protein molecule volume analysis [34]. Standard Voronoi methods fix a discrete sets of points (e.g. the nuclei's barycenters) as the centers of tessellation, returning polygonal regions delimited by a number of edges dependent on the number and distribution of the nearest centers; in case the centers are few and regularly distributed, the polygonal regions are simple and delimited by few straight edges, as in the example of Fig. 1.b. Although the reference nuclei are the same as for standard Voronoi, the tessellation method used in our technique calculates distances from a set of smoothed curves rather than from individual centers, thus returning complex-shaped profiles that are a more realistic approximation of the cellular membranes (see Fig. 1.c for examples).

In our tessellation approach the *minimum distance* criterion from nuclear boundaries is exploited as follows (see Fig. 2): the image is partitioned in as many regions as the number of nuclei in the tissue. These regions are initialized by the set of pixels bounded by the nuclear membranes and are univocally identified by a region-label (see Fig. 2.a). Then a *labelling procedure* assigns each pixel in the image to one of the regions; in particular each pixel is given a region-label depending on the minimum distance between that pixel and the membranes of the surrounding nuclei, so that the pixel is finally assigned to the region having the closest nucleus in it (see Fig. 2.b). Approximate cellular membranes are then obtained by outlining the boundaries of the final regions (see Fig. 2.c-d).

The labelling process is based on detecting for each pixel in the image the closest nucleus, which requires to compute distances between points and nuclear membranes' profiles. Since a typical cancer tissue image may contain several hundreds of nuclear membranes with highly irregular profiles, this task may be computationally very intensive. In order to speed up this process we implemented an optimized procedure which detects the closest nucleus to a given input point in the image in two sequential steps. In the first step we perform a nearest-neighbours search to find the set of n nuclei closest to the input point. In particular we approximate the nuclear membranes with their minimum bounding rectangles and we select the closest n nuclei based on the Euclidean distance between the input point and the vertices of the rectangles. See Section 3 for details about parameter n. In the second step we select the closest nucleus among the previous n, this time based on

the Euclidean distances calculated between the input point and *all* the points of nuclear membrane's profile. Therefore the computation of Euclidean distance between points and curves is limited to a small number of nuclei in the image, thus decreasing significantly the computational complexity of the labelling process.

2.2 Detection of final cellular membranes

The main steps of the final cellular membranes' detection are summarized by Fig. 3, where the approximate cell membrane and the final cellular membrane are represented in yellow and in red, respectively: *i)* in the stained portions (labelled by *a*) we compute the red membrane as the barycenter curve of the brown-colored area; *ii)* at fork regions of the brown membrane (labelled by *b*) we force the red membrane to lie on the path that is closer to the nucleus of the cell through specific weighting coefficients in the barycenter's equation; *iii)* in the unstained portions of the membrane (labelled by *c*) we force the red membrane to coincide with the approximate cell membrane; *iv)* we refine the connection of the stained and the unstained portions by calculating a best fitting curve and removing outliers.

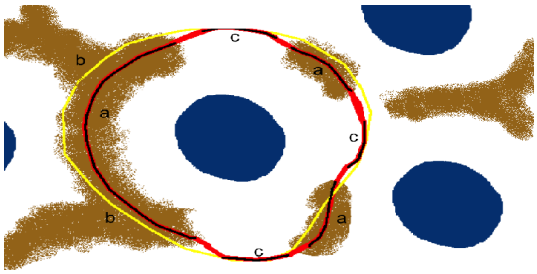

Figure 3: Scheme of detection of final cellular membranes. The final membrane is computed as the barycenter curve of the brown-colored area (a) and forced to lie on the path that is closer to the nucleus in order to handle forks (b). In the unstained regions the final membrane is forced to coincide with the approximate cell membrane, in yellow (c). Stained and unstained tracts of the final membrane are connected by a best fitting curve, in red.

A detailed description of the procedure is provided as follows.

First of all, reactive membranes are detected through color filtering, highlighting the only brown colored areas in the image. For this purpose, we used a specific color deconvolution algorithm [35] that was shown to achieve better results than other color segmentation methods, especially in IHC applications [12]. This method allows the separation not only of H and DAB (as in the case presented in this paper) but of all the standard histological stains (e.g. H-E, H AEC, etc.) as well as of any other stains, provided that their RGB vectors are experimentally determined and given as an input to the method (see [35], [12] for details).

Then brown-colored membranes are connected to the approximate cell membranes in the non-reactive regions. For this purpose, the area across the approximate membrane, whose width w in pixels depends on image resolution (see Section 3 for details), is scanned by a scan line having one end on the pixel at the center of the nucleus and the other one on the pixel at the external border of the scanned area. (see Fig. 4); the cellular membrane is then reconstructed one pixel at a time as the weighted barycenter B of the brown pixels among the scan line, as in the following equation:

$$B = \frac{\sum_j c_j I_j j}{\sum_j c_j I_j}, \tag{1}$$

where j is the pixel's coordinate along the scan-line. This coordinate is 0 on the approximate membrane, negative in the inner part of the scanned area and positive in the outer part. I_j is the intensity value of pixel j, calculated as the complementary of the average RGB values and c_j is a coefficient for barycenter computation, calculated as follows:

$$c_j = \begin{cases} 1 & if \quad j \leq 0 \\ 1 - kj & if \quad j > 0 \end{cases} \tag{2}$$

where k is a coefficient experimentally tuned (see Section 3 for details).

As shown in (2), c_j is equal to 1 for pixels with negative coordinate (i.e. closer to nucleus with respect to the approximate membrane); on the contrary, for pixels with positive coordinate c_j decreases linearly as the coordinate (i.e. the distance from the nucleus of the cell) increases. In this way, when the brown stain forks the membrane contour is forced to follow the path closest to the nucleus.

The intensity values of the background pixels are set to 0, whereas the intensity values of the scan-line's pixels that belong to or touch the approximate membrane are set to 1. In this way, in absence of brown pixels along the scan-line, the barycenter B is forced to lie on the approximate membrane. As a consequence, the final cellular membrane coincides with the approximate membrane in the non-reactive (unstained) regions of

the tissue. On the contrary, in the reactive regions of the tissue, brown pixels have intensity values much higher than 1 (ranging from 70 to 255), which always prevails in the computation of the barycenter. Therefore the final cellular membrane is forced to lie on the pixels where the brown stain is more intense. Fig. 4 shows a picture of the *scanning procedure*.

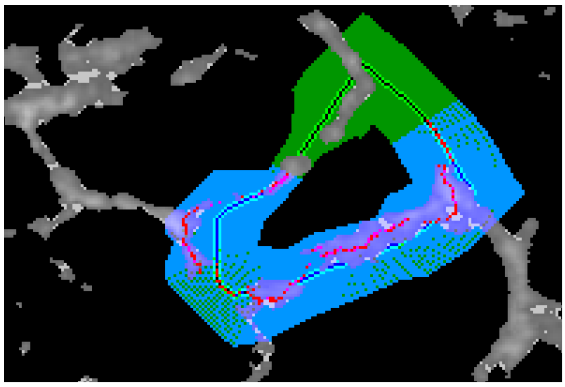

Figure 4: Trace of scanning procedure. Non reactive regions which are not of interest are shown in black; reactive brown-colored membranes are shown in gray; the area scanned by the scan-line is shown in blue and green (in blue regions already scanned, in green regions to be scanned). In the middle of this area there is the approximate cellular membrane. At each scanning step the barycenters of the brown pixels along the scan-line are computed. These barycenters, that compose the contour of the final cellular membrane, are shown in red. In the non-reactive regions the final cellular membrane is forced to coincide with the approximate membrane.

(a) (b) (c)

Figure 5: Example of membranes detection on *non-small cell lung carcinoma* (NSCLC) tissue immunohistochemical image. The final cellular membranes provided by our automated technique are highlighted in blue

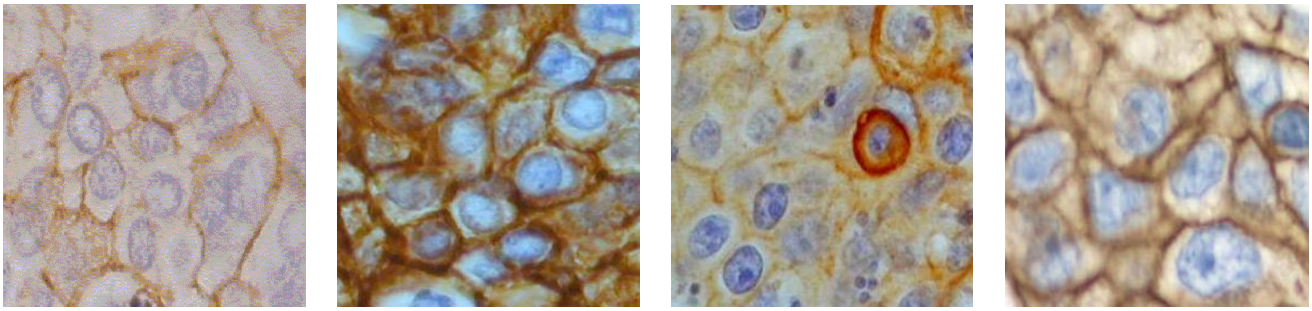

Figure 6: Examples of immunohistochemical images used to validate our method (details).

The second step of final cellular membranes' segmentation after the *scanning procedure* consists of an *iterative fitting procedure* which refines the connection between stained and unstained tracts of the cellular membrane and iteratively deletes *outlier* pixels in the curve, which may be present due to local inhomogeneities of the brown stain. Outliers are pixels whose distance from the best fitting curve is more than three times the standard deviation, as in the traditional definition in statistics [36]. After removing the outliers, third-degree polynomial fitting is applied. Examples of final cell membrane detection are shown in Fig. 5.

3 Implementation

The algorithm has been implemented in C++ inheriting the whole class hierarchy of the open-source *Cimg* public library [37]. The main parameters' values are reported in Table 1. The width w of the area of the *scanning procedure* (see Section 2.2) is related to the thickness of membrane staining in chromogenic IHC images; its value has been derived from the pathologists' observations and it is provided in μm in order to be resolution-independent. The number of nuclei n in the nearest-neighbours search for the calculation of the distances between points and nuclear membranes' profiles (see the *labelling procedure* in Section 2.1) was tuned in order to speed up the procedure for approximate cell membranes' computation without compromising the accuracy of membranes' approximation. Finally, the coefficient k of (2) (see *scanning procedure* for the detection of final cellular membranes in Section 2.2) was empirically tuned in order to handle forks of the cellular membrane's profile and does not have to be adjusted by the user. All the values of the parameters reported in Table 1 are independent from image resolution as well as from image content.

Table 1: Parameters' and coefficients' values.

Parameter	value
number of nuclei in nearest neighbour search (n)	4
width of the scanned area (w)	5.5 μm
coefficient of equation (2) (k)	0.0018

4 Experimental Results and Discussion

We tested our membrane segmentation technique for computer-aided protein activity quantification on eight datasets of real IHC images showing membrane stained cancer tissues from different anatomical locations, including lung (Non Small Cell Lung Carcinoma, NSCLC), prostate and liver tissue. The eight datasets showed tissue specimens extracted from different patients and stained by H-DAB (see Fig. 6 for examples), including almost 400 cells. The images were acquired through brightfield digital microscopy at different enlargements; a complete characterization of the datasets, including the IHC score as provided by a pathologist according to the standard guidelines reported in [27], is provided in Table 2.

Table 2: Characterization of the validation datasets.

dataset	tissue	IHCscore	resolution	size	cells
1	lung	2+	0.6 μm/px	541x210	116
2	lung	2+	0.3 μm/px	279x237	38
3	lung	1+	0.3 μm/px	202x293	50
4	lung	1+	0.15 μm/px	345x236	27
5	lung	3+	0.3 μm/px	249x274	31
6	lung	1+	0.15 μm/px	507x609	46
7	liver	3+	0.4 μm/px	259x277	63
8	prostate	3+	0,15 μm/px	566x306	25

We had all the cellular membranes in our datasets manually traced by a pathologist and we used manual segmentations as the ground truth to validate our segmentation method. We performed both a *direct validation* based on a pixel-wise distance metric between the automated and manual membranes and an *indirect validation* based on the concordance between protein expression measures obtained from automated and manual membranes.

The *direct validation* is based on the computation of the *Hausdorff distance* [38], a well-known distance metric that measures the proximity between two sets of points by calculating the maximum distance between the first set and the nearest point of the second set: it is a severe metric that takes into account the maximum span between the two trajectories, instead of the average distance; moreover it has been already used to validate membrane segmentation accuracy [18]. In our experiments we calculated the *Hausdorff distance* between each automated membrane and the corresponding manual membrane, as follows:

$$d_H(A,M) = max(\sup_{a\in A}\inf_{m\in M} d(a,m), \sup_{m\in M}\inf_{a\in A} d(a,m)), \tag{3}$$

where a and m are respectively the pixels belonging to the automated membrane A and the manual membrane M, and $d(a,m)$ is the Euclidean distance between a and m.

The results obtained in each validation dataset are reported in the boxplots of Fig. 7. It is a widely used representation technique in descriptive statistics where the boxes have horizontal lines at the three data distributions quartiles (the median value is highlighted in red) and the vertical dotted lines show the extent of the data distribution.

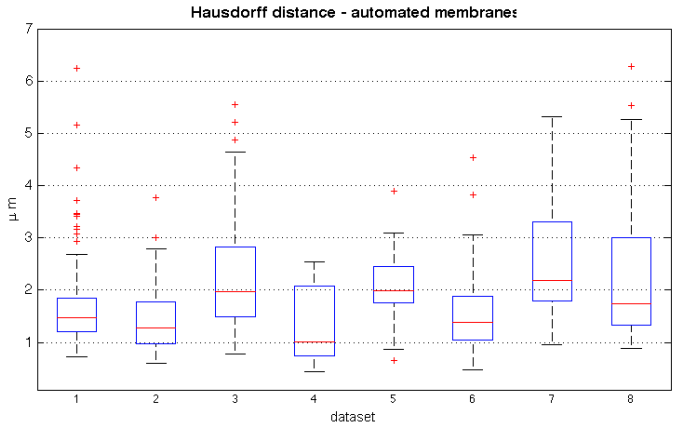

Figure 7: Boxplot of Hausdorff distances between automated and manual membranes.

We obtained distances between automated and manual membranes with a median value spanning between 1 and 2.2 μm, and with a mean standard deviation of 0.95 μm.

For a correct interpretation of the results, the intrinsic variability of the ground truth should be taken into account. In fact, the Hausdorff distance is extremely influenced by localized variations of the curve, which makes it a good metric of segmentation accuracy, provided that the reference curve is reliable enough. Therefore it works well for applications where the manual operator is able to identify and trace the trajectory of cellular membranes with a high precision, as in [18]. In the specific applicaton of chromogenic IHC, on the contrary, the Hausdorff distance may be strongly biased by the subjectivity and variability of the manual tracement. The reason of this variability is twofold: i) in the stained portions of the tissue, the brown stain can be diffused over a large area over the cellular membrane, about 1-1.5 μm thick (see Fig. 8, cell 1, as an example); ii) in the unstained portions of the tissue, the membranes are not visible; as a consequence, the manual tracement, besides being a realistic approximation derived from the experience of the pathologist, may be even more variable (see Fig. 8, cell 2).

In order to evaluate the variability of manual segmentations and its influence on the Hausdorff measure, we asked several operators (fifteen) to manually trace the cellular membranes of two sample cells, the former one with a well-delineated cellular membrane and the latter with a mostly unstained cellular membrane (shown in Fig. 8). Then we calculated the Hausdorff distance between each couple of manually traced membranes, and reported the results in the boxplots of Fig. 8.

We obtained that manual measurements had a median Hausdorff distance of 1 μm and 1.9 μm respectively in the stained and unstained cell, with standard deviations of 0.57 and 0.97 μm, which shows that the intrinsic variability of manual segmentations is comparable with the variability of the segmentations provided by our proposed automated approach.

Since we verified that the pixel-wise evaluation is extremely biased by the variability of the manual tracement, especially in the unstained tracts, in our experiments we exploited also an *indirect validation* that relies on the concordance between the protein expression evaluated along automated and manually traced membranes, respectively. This metric does not rely on a pixel-by-pixel coincidence of the two trajectories and therefore it is less influenced by the intrinsic variability of the manual membrane; nevertheless, it is the best indicator of the similarity of the automated and manual membrane in the context of immunohistochemical analysis, which is the main target of membrane segmentation.

According to the recent guidelines by [27], membrane stained tissues are assigned a IHC score (from 0 negative to 3+ positive) depending on the overall intensity of the stain and on the *staining continuity* along the membrane. The latter feature, which is computed as the percentage of stained pixels along the cellular membrane (i.e. number of stained pixels divided by total number of pixels), is highly dependent on membrane segmentation: thus, in our work we used staining continuity as an indirect indicator of membrane segmentation accuracy.

More specifically, for each dataset we performed a linear regression between measurements of *staining continuity* computed respectively along automated and manually traced membranes (taken as a reference) and we evaluated the statistical significance of the regression coefficient through *Student's t-test* [39]. Then we computed the average error (E_{AVG}) and the root mean square error (E_{RMSE}) incurred by our automated approach

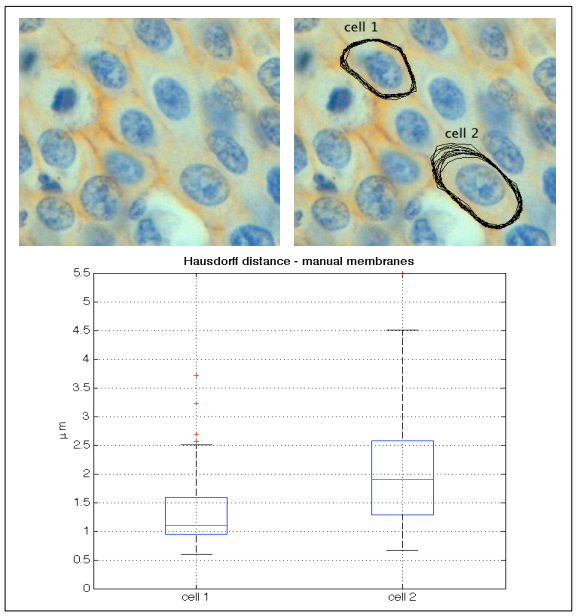

Figure 8: Variability of manual-trace membranes in two sample cells, the former with diffused brown staining (cell 1), the latter with unstained membrane (cell 2). The manual tracements provided by fifteen operators are shown in black superimposed on the original image; the Hausdorff distances between each couple of manual-trace curve are reported in the boxplots below the images.

with respect to ground truth consisting on the same measurements of staining continuity along manual-trace membranes, as follows:

$$E_{AVG} = \frac{1}{N} \sum \mid c_{auto} - c_{manual} \mid \tag{4}$$

$$E_{RMSE} = \sqrt{\frac{1}{N} \sum (c_{auto} - c_{manual})^2}, \tag{5}$$

where c_{auto} and c_{manual} are the staining continuity calculated along automated and manual membranes, respectively, and N is the number of cellular membranes of the dataset.

Moreover we computed the coefficient of correlation between the two sets of measurements by dividing the covariance of the two variables c_{auto} and c_{manual} by the product of their standard deviations, as reported in the following equation:

$$\rho_{auto,manual} = \frac{Cov(auto, manual)}{\sigma_{auto} \cdot \sigma_{manual}} \tag{6}$$

This validation procedure evaluates the statistical equivalence of the two variables c_{auto} and c_{manual} and quantifies the statistical significance of this equivalence; the statistical equivalence of the two variables is an indirect indicator of the accuracy of membrane segmentation.

The results obtained in each validation dataset are reported in Table 3: in particular, the second column reports the coefficient of correlation between automated and manual-trace measurements as in (6); third and fourth columns report the coefficient of the linear regression line and its region of statistical deviation with a 99% confidence level, respectively. The last two columns report the average of differences between automated and manual-trace measurements (namely, average error) and the root mean square error (RMSE), respectively, calculated as in 4 and 5.

As shown in Table 3, we obtained similar results in all the tested datasets. In particular we found that our automated measurements were highly correlated with manual-trace measurements, with average coefficient of correlation 0.95. Moreover we proved that automated and manual measurements were linearly correlated, with a regression coefficient close to 1 in six datasets out of eight and close to 0.9 in the remaining two datasets, and a narrow range of deviation. Average and root mean square error with respect to manual measurement of staining continuity were below 3.82 and 5.80% respectively, which is much below the resolution achievable by visual evaluation.

At last, we obtained that automated and manual-trace measurements were statistically equivalent in each of the validation datasets. This was proved by performing *Student's t-tests* on the difference between the two samples with a 99% confidence level.

As it is shown by the examples reported in Fig. 5, the segmentations provided by our automated technique are accurate. Minor deviations from the stained boundary may arise due to local superposition of the reference nuclei

Table 3: Experimental results on computation of staining continuity along cellular membranes.

dataset	Corr Coeff	Regr Coeff	Accept Reg	Av Err	RMSE
1	0.99	0.97	± 0.34	0.38	3.29
2	0.98	0.96	± 0.096	0.14	2.68
3	0.88	0.94	± 0.20	2.57	5.64
4	0.98	0.96	± 0.108	0.77	3.3
5	0.97	0.85	± 0.11	0.25	1.58
6	0.98	0.96	±0.09	0.04	4.00
7	0.94	0.88	±0.12	3.82	5.80
8	0.90	1.02	±0.36	0.09	5.35

with the target membrane or due to missing reference nuclei (e.g. left tract of cell in Fig. 5(c)); these artifacts may be generated by the superposition of different tissue layers, diffusion of the dye partially or completely hiding the nuclei and tissue deformations happening during the preparation of the sample. Nevertheless, our quantitative validation demonstrates that our technique copes well with all the issues of IHC segmentation and provides results that are statistically comparable with manual segmentations.

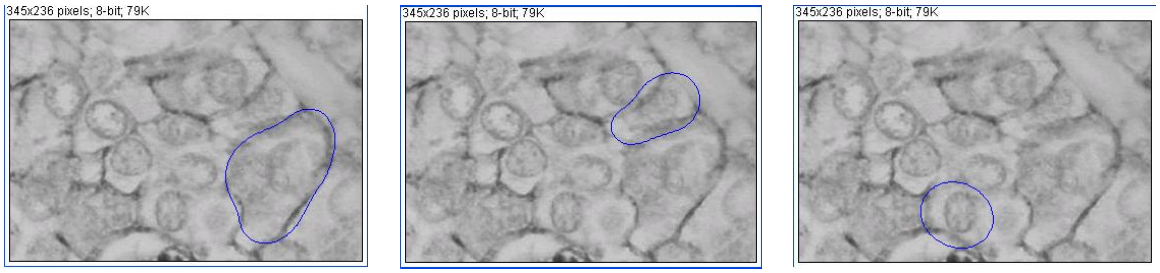

(a) (b) (c)

Figure 9: Example of membranes detection using active contours approach.

In order to compare the results obtained by our technique with other popular automated approaches, we made additional experiments with active contours, a well established segmentation method in Computer Vision as well as in medical imaging that addresses gradient as well as spatial intensity information [29]. Active contours have the inherent capability of modelling the target object through a closed curve: thus they overcome the problem of connecting broken contour lines, that is a major limitation in other widespread edge-based or region-based segmentation techniques. In fact, as anticipated in Section 1 several formulations of active contours have been applied to the task of cell segmentation. Nevertheless, active contours' performance is extremely affected by curve initialization, as well as by heterogeneous staining and presence of foreign particles in the tissue which may attract the curve far from the target membrane.

In this work, we implemented a semi-automated segmentation technique using the active contours presented by [41], that were initialized by an operator close to the targeted cellular membranes. Moreover, in order to decrease the influence of wrong curve attractors in the images, we preventively performed both noise and color-filtering. More details about the implementation of the active contours for IHC image segmentation are provided in our previous work [31]. We run experiments in a lung cancer tissue dataset, measuring the performance of the automated segmentation versus manual segmentation through the aforementioned indirect validation based on the staining continuity. The results obtained by active contours approach and the results obtained in the same dataset by our automated technique are reported in Table 4 for comparison.

Table 4: Experimental results on computation of staining continuity along cellular membranes in a lung cancer tissue sample. The results obtained by active contours and by our proposed technique are reported in the first and second row, respectively.

	Corr Coeff	Av Err	RMSE
active contours	0.629	23.44	26.44
proposed	0.98	0.14	2.68

In Fig. 9 we show examples of cell membrane detection obtained by active contours approach. The segmentation provided by our proposed method on the same cellular membranes was already shown in Fig. 5. The superiority of our method over active contours approach is fairly evident from the quantitative results as well as from visual evaluation.

5 Conclusions

We presented a fully-automated membrane segmentation approach that allows the quantification of the expression of membrane receptors in cancer tissue images, which is usually performed by pathologists via visual inspection of the samples. Our techniques streamlines this error-prone and time-consuming process, thereby facilitating analysis and diagnosis as well as the design of novel targeted therapies. The automated segmentation of cellular membranes as provided by our method leads to the analysis of membrane protein activity in situ on a cell-by-cell basis, which is critical for the accurate assessment of a number of important pathologies; moreover it allows any other application that relies on accurate tissue and cell exploration in IHC tissue images. In particular, our technique overcomes the limitations of traditional segmentation techniques based on local or spatial intensity information as well as gradient magnitude variation. The effectiveness and robustness of the proposed method has been tested on real immunohistochemical images from several tissue locations, including lung, prostate and liver tissue. Results of comparison with ground truth provided by pathologists on several real-life datasets demonstrate the high accuracy of our approach in the context of IHC analysis.

6 Acknowledgements

The authors acknowledge Dr. Marco Volante and his collaborators of Hospital S. Luigi of Orbassano, Torino, Italy for providing the images and as well as for the helpful discussion.

References

[1] T.K. Taneja, and S.K. Sharma "Markers of small cell lung cancer" *World Journal of Surgical Oncology*, Vol(2):10, 2004

[2] Z. Ahmed, N.S. Azad, Y. Bhurgari, R. Ahmed, N. Kayani, S. Pervez, and S. Hasan "Significance of immunohistochemistry in accurate characterization of malignant tumors" *J Ayub Med Coll Abbottabad*, Vol18(2):38-43, 2006

[3] Z. Theodosiou, I.N. Kasampalidis, G. Livanos, M. Zervakis, I. Pitas, and K. Lyroudia "Automated Analysis of FISH and Immunohistochemistry Images: a Review" *Cytometry A*, Vol71A:439-450, 2007

[4] M.J. Borad, R. Penny, M. Bittner, J. Gardner, S. Shack, E. Campbell, D. Taverna, R. Love, J. Trent, and D. Von Hoff "Molecular Profiling Using Immunohistochemistry (IHC) and DNA Microarray (DMA) as a Tool to Determine Potential Therapeutic Targets in Patients who Have Progressed on Multiple Prior Therapies" *1st AACR Int Conf on Molecular Diagnostics in Cancer Therapeutic Development* 2006

[5] M. Cregger, A.J. Berger, and D.L. Rimm "Immunohistochemistry and Quantitative Analysis of Protein Expression" *Arch Path Lab Med*, Vol130(7):1026-1030, 2006

[6] M. Lacroix-Triki, S. Mathoulin-Pelissier, J. Ghnassia, G. Macgrogan, A. Vincent-Salomon, V. Brouste, M. Mathieu, P. Roger, F. Bibeau, and J. Jacquemier "High inter-observer agreement in immunohistochemical evaluation of HER-2/neu expression in breast cancer: A multicentre GEFPICS study" *EJC*, Vol42(17):2946-2953, 2006

[7] J.P. Sloane, I. Amendoeira, N. Apostolikas, J.P. Bellocq, S. Bianchi, W. Boecker, G. Bussolati, D. Coleman, CE.Connolly, P. Dervan, V. Eusebi, C. De Miguel, M. Drijkoningen, C.W. Elston, D. Faverley, A. Gad, J. Jacquemier, M. Lacerda, J. Martinez-Penuela, C. Munt, J.L. Peterse, F. Rank, M. Sylvan, V. Tsakraklides, B. Zafrani "Consistency achieved by 23 European pathologists in categorizing ductal carcinoma in situ of the breast using five classifications. European Commission Working Group on Breast Screening Pathology" *Hum Pathol*, Vol 29:1056-1062, 1998

[8] K.A. Divito, and RL. Camp "Tissue Microarrays - Automated Analysis and Future Directions" *Breast Cancer Online*, Cambridge University Press, Vol8(7) 2005

[9] M.G. Rojo, G. Bueno, and J. Slodkowska "Review of imaging solutions for integrated quantitative immunihistochemistry in the pathology daily practice" *Folia Histochem Cytobiol* Vol47(3):349-354, 2009.

[10] C.R. Taylor, and R.M. Levenson "Quantification of immunohistochemistry - issues concerning methods, utility and semiquantitative assessment II" *Histopathology*, Vol 49:411-424, 2006

[11] E.M. Brey, Z. Lalani, C. Johnston, M. Wong, LV. McIntire, PJ. Duke, and CW. Patrick Jr. "Automated Selection of DAB-labeled Tissue for Immunohistochemical Quantification" *The Journal of Histochemistry and Cytochemistry*, Vol51(5):575-584, 2003

[12] A. Ruifrok, R. Katz, and D. Johnston "Comparison of Quantification of Histochemical Staining by Hue-Saturation-Intensity (HSI) Transformation and Color Deconvolution" *Applied Immunohistochemistry and Molecular Morphology*, Vol(11):1, 2004

[13] N. Malpica C.O. de Solrzano, IJ. Vaquero, A. Santos, I. Vallcorba, J.M. Garca-Sagredo, and F. del Pozo "Applying Watershed Algorithms to the Segmentation of Clustered Nuclei" *Cytometry*, Vol(28):289-297, 1997

[14] L. Yang, P. Meer, and D.J. Foran "Unsupervised Segmentation Based on Robust Estimation and Color Active Contour Models" *IEEE Transactions on Information Technology in Biomedicine*, Vol(9):3, 2005

[15] D.P. Mukherjee, N. Ray, and S.T. Acton "Level Set Analysis for Leukocyte Detection and Tracking" *IEEE Transaction on Image Processing*, Vol. 13(4), 2004

[16] A. Elmoataz, S. Schupp, R. Clouard, P. Herlin, and D. Bloyet "Using active contours and mathematical morphology tools for quantification of immunohistochemical images" *Signal Processing*, Vol(71):215-226, 1998

[17] T.R. Jones, A. Carpenter and P. Golland "Voronoi-Based Segmentation of Cells on Image Manifolds" *LNCS* Vol 3765: 535-543, 2005

[18] C. Zanella, M. Campana, B. Rizzi, C. Melani, G. Sanguinetti, P. Bourgine, K. Mikula, N. Peyrieras, and A. Sarti "Cells segmentation from 3-D confocal images of early zebrafish embryogenesis" *IEEE Trans Image Process.* Vol 19(3): 770-81, 2010

[19] J. Han, H. Chang, K. Andarawewa, P. Yaswen, M.H. Barcellos-Hoff, and B. Parvin 'Multidimensional profiling of cell surface proteins and nuclear markers" *IEEE/ACM Trans Comput Biol Bioinform.* Vol 7(1): 80-90, 2010

[20] T. Markiewicz, C. Jochymski, R. Koktysz, and W. Kozlowski "Automatic cell recognition in immunohistochemical gastritis stains using sequential thresholding and SVM network" *5th IEEE International Symposium on Biomedical Imaging (ISBI 2008)*, 971-974, 2008

[21] P. Phukpattaranont, and P. Boonyaphiphat "Computer-aided analysis of nuclear stained breast cancer cell images" *5th International Conference on Electrical Engineering/Electronics, Computer, Telecommunications and Information Technology (ECTI-CON 2008)*, Vol1:485-488, 2008

[22] C. Hang, R.A. DeFilippis, T.D. Tlsty, and B. Parvin "Scoring histological sections through immunohistochemistry" *5th IEEE International Symposium on Biomedical Imaging (ISBI 2008)*, 344-347, 2008

[23] C. Sun, P. Vallotton, D. Wang, J. Lopez, Y. Ng and D. James "Membrane boundary extraction using circular multiple paths" *Pattern Recognition*, Vol42(4):523-530, 2009

[24] D. Baggett, M.A. Nakaya, M. McAuliffe, TP. Yamaguchi, and S.Lockett "Whole Cell Segmentation in Solid Tissue Sections" *Cytometry* Part A 67A:137-143, 2005

[25] M.A. Gavrielides, H. Masmoudi, N. Petrick, K.J. Myers, and S.M. Hewitt "Automated evaluation of HER-2/neu immunohistochemical expression in breast cancer using digital microscopy" *5th IEEE International Symposium on Biomedical Imaging (ISBI 2008)*, 808-811, 2008

[26] H. Masmoudi, S.M. Hewitt, N.Petrick, K.J.vMyers, and M.A.vGavrielides "Automated quantitative assessment of HER-2/neu immunohistochemical expression in breast cancer" *IEEE Transactions on Medical Imaging*, Vol. 28(6):916-25, 2009

[27] . A.C.Wolff, M.E. Hammond, J.N. Schwartz, K.L. Hagerty, D.C. Allred, R.J. Cote, M. Dowsett, P.L. Fitzgibbons, W.M. Hanna, A. Langer, L.M. McShane, S. Paik, M.D. Pegram, E.A. Perez, M.F. Press, A. Rhodes, C. Sturgeon, S.E. Taube, R. Tubbs, G.H. Vance, M. van de Vijver, T.M. Wheeler, and D.F. Hayes "American Society of Clinical Oncology/college of American Pathologists guideline recommendations for human epidermal growth factor receptor 2 testing in breast cancer" *Arch. Pathol. Lab. Med.*, Vol. 131:18-43, 2007

[28] J.B.T.M. Roerdink and A. Meijster "The Watershed Transform: Definitions, Algorithms and Parallelization Strategies" *Fund Inform*, Vol. 41:187-228, 2001

[29] M. Kass, A. Witkin, and D. Terzopoulos "Snakes: active contours models" *Int'l J Comp Vis*, Vol. 1(4):321-331, 1987

[30] S. Di Cataldo, E. Ficarra, and E. Macii "Selection of Tumor Areas and Segmentation of Nuclear Membranes in Tissue Confocal Images: a Fully-Automated Approach" *IEEE Int. Conf. on Bioinformatics and Biomedicine (BIBM2007)*, Fremont, 390-398, 2007

[31] S. Di Cataldo, E. Ficarra, A. Acquaviva, and E. Macii "Segmentation of Nuclei in Cancer Tissue Images: Contrasting Active Contours with Morphology-Based Approach" *IEEE 8th Symposium on Bioinformatics and Bioengineering (BIBE2008)*, Athens, 1-6, 2008

[32] F. Aurenhammer, and R. Klein "Voronoi Diagrams" *Handbook of Computational Geometry*, (Ed. J.-R. Sack and J. Urrutia), Amsterdam, Netherlands: North-Holland, Ch. 5, pp. 201-290, 2000

[33] K. Fukuda,"Frequently Asked Questions in Polyhedral Computation" http://www.ifor.math.ethz.ch/ fukuda/polyfaq/polyfaq.html

[34] A.R. Kansal, and T.S. Deisboeck "Simulated Brain Tumor Growth Dynamics Using a Three-Dimensional Cellular Automaton" *Journal of Theoretical Biology*, Vol.203(4):367-382, 2000

[35] A.C. Ruifrok, and DA. Johnston "Quantification of Histochemical Staining by Color Deconvolution" *Anal Quant Cytol Histol*, Vol. 23(4):291-299, 2001

[36] P. Sun, and S. Chawla "On Local Spatial Outliers" *IEEE Int Conf Data Mining ICDM04*, 209-216, 2004

[37] D. Tschumperl "The Cimg Library" http://cimg.sourceforge.net

[38] J. Munkres "Topology" , Prentice Hall, 2nd edition, 280-281, 1999

[39] J.H. Zar "Biostatistical analysis" 4th edition. Prentice Hall, Upper Saddle River, NJ, 1999

[40] R.C. Gonzalez, and R.E. Woods "Digital Image Processing" 3rd edition. Prentice Hall,Upper Saddle River, NJ, 2007

[41] M. Jacob, T. Blu, and M. Unser "Efficient Energies and Algorithms for Parametric Snakes" *IEEE Transactions on Image Processing*, Vol. 13(9):1231-1244, 2004